

Latest results on cosmic rays light elements with the CALorimetric Electron Telescope (CALET) on the International Space Station

Francesco Stolzi^{a,b,*} for the CALET collaboration

^a*Department of Physical Sciences, Earth and Environment,
University of Siena, via Roma 56, 53100 Siena, Italy*

^b*INFN Sezione di Pisa,
Polo Fibonacci, Largo B. Pontecorvo, 3, 56127 Pisa, Italy*

E-mail: francesco.stolzi@unisi.it

The CALorimetric Electron Telescope (CALET) is an experiment installed on the International Space Station designed to carry out precision measurements of high energy cosmic-rays (CR) with the aim of investigating their origin, the mechanisms of acceleration and galactic propagation, and the presence of possible nearby astrophysical CR sources. The instrument combines a scintillator hodoscope for charge identification, thin imaging scintillating fiber calorimeter for particle tracking and complementary charge measurement, and total absorption PWO calorimeter for energy measurement. CALET is able to obtain precise measurements of the fluxes of CR electrons and γ rays up to TeV region, the energy spectra of CR nuclei from proton to nickel from few tens of GeV to hundreds of TeV and secondary-to-primary ratios of elements up to $Z = 40$. Here we present the highlights of CALET observation of light elements carried out during the first seven years of operation, including a direct measurement of the electron+positron spectrum from 11 GeV to 4.8 TeV and proton spectrum from 50 GeV to 60 TeV. Results on the electromagnetic counterpart search for LIGO/Virgo gravitational wave events and gamma-ray bursts are also summarized.

*Multifrequency Behaviour of High Energy Cosmic Sources XIV (MULTIF2023)
12-17 June 2023
Palermo, Italy*

*Speaker

1. Introduction

The CALorimetric Electron Telescope (CALET) is a space-based experiment on the ISS, optimized for the measurement of the all-electron spectrum. The instrument was launched on August 19, 2015, and installed on the JEM EF (Japanese Experiment Module Exposed Facility) on the ISS. Scientific observations [1] started on October 13, 2015, and smooth and continuous operations have taken place since then. The objectives of the CALET mission include the investigation of CR origin and the mechanisms of acceleration and galactic propagation, the possible presence of nearby astrophysical CR sources and the nature of dark matter. Thanks to its capability of identifying cosmic rays with individual element resolution, CALET is not only able to obtain precise measurements of the electron + positron flux, but also carrying out direct measurements of the spectra and relative abundances of light and heavy cosmic nuclei, from proton to nickel, up to TeV region. The abundances of trans-iron elements up to $Z \sim 44$ are studied with a dedicated program. Monitoring the gamma ray sky from 1 GeV up to 10 TeV, CALET can obtain information including properties of the Galactic diffuse gamma rays and spectra of bright Galactic point sources. CALET also has the possibility to detect a prompt emission and high energy gamma-ray emission of short GRBs associated with binary neutron star merger searching for electromagnetic counterparts of the gravitational waves.

2. The CALET instrument

CALET is made of a main detector, the CALorimeter and a second detector the Gamma-ray Burst Monitor (CGBM). The CAL is based on a thick calorimetric instrument (30 radiation lengths), designed to achieve electromagnetic shower containment and a large proton rejection capability ($> 10^5$). It is longitudinally segmented into a fine grained imaging calorimeter (IMC) followed by a total absorption calorimeter (TASC). The IMC is a sampling calorimeter segmented longitudinally into 16 layers of scintillating fibers, readout individually, and interspaced with thin tungsten absorbers. It can reconstruct the incident direction of cosmic rays. The particle's energy is measured with the TASC, a $27 X_0$ thick homogeneous calorimeter with 12 alternate X-Y layers of lead-tungstate (PWO) logs. The charge identification of individual nuclear species is performed by the Charge Detector (CHD), a two-layered hodoscope of plastic scintillators at the top of the apparatus. It identifies the charge from $Z = 1$ to $Z = 40$ with excellent resolution, from 0.1 for protons to ~ 0.3 for iron (in charge unit). An independent charge measurement, via multiple samples of specific energy loss (dE/dx) in each fiber is also provided by IMC up to the onset of saturation which occurs for ions more highly charged than silicon. The CGBM, which consists of two kinds of scintillation detectors, Hard X-ray Monitor (HXM) and Soft Gamma ray Monitor (SGM), is able to observe GRBs and other X-ray, gamma-ray transients. CGBM has been monitoring the sky with X-rays and gamma rays in the energy range from 7 keV to 20 MeV.

3. Flight operations and calibrations

The CALET observation campaign started on October 13th, 2015. Since then the instrument has been taking science data continuously with remarkable performance and stability. As of May

2023, CALET collected more than 3.9 billion events above 1 GeV with a total observation time of more than 2770 days and a live time fraction $\sim 85\%$ of the total time. The high-energy (HE) trigger mode, designed to maximize the collection power for electrons above 10 GeV and other high-energy shower events, allows to reach an exposure of $250 \text{ m}^2 \text{ sr day}$. Calibration and test of the instrument took place at the CERN-SPS during five campaigns between 2010 and 2015 with beams of electrons, protons, and relativistic ions. The TASC response was studied at CERN SPS in 2015 using a beam of accelerated ion fragments with $A/Z = 2$, obtained with a primary beam of ^{40}Ar nuclei, and kinetic energy of 13, 19 and 150 GeV/ c/n [2]. Each channel of CHD, IMC, and TASC was calibrated using penetrating proton and He particles selected in-flight by a dedicated trigger mode. Raw signals are corrected for light output non-uniformity, gain differences among the channels, position and temperature dependence, as well as temporal gain variations. The four gain ranges of each TASC channel are calibrated with flight data and stitched together to provide a seamless response spanning more than six orders of magnitude, from 1 GeV to 1 PeV.

4. Results

4.1 Precision Measurement of the Electron Spectrum

CALET is optimized for the measurement of the all-electron spectrum. Thanks to the $30 X_0$ -thick calorimeter it can fully contain the electron showers up to the TeV scale with an excellent energy resolution ($<2\%$ above 20 GeV). Proton showers of equivalent energy deposit undergo a larger energy leakage from the bottom layers of the TASC. This feature is used to separate electrons from protons exploiting the TASC and IMC capability to image the longitudinal and lateral profiles of electromagnetic and hadronic cascades. Electrons are identified using a simple two-parameter cut and a multivariate analysis based on boosted decision trees (BDTs). The residual contamination of protons is $\sim 5\%$ up to 1 TeV, and $10\% - 20\%$ in the 1 - 4.8 TeV region, keeping a constant high efficiency of 80% for electrons. The electron + positrons flux presented at this workshop and shown in Fig.1 is based on 1815 days of flight data collected with the high-energy shower trigger. It corresponds to an increase by a factor of 2.3 of the available statistics with respect to the latest CALET all-electron spectrum publication [3]. The flux cover an energy range from 11 GeV to 4.8 TeV. The vertical error bars represent the statistical errors, while the gray band represents the quadrature sum of statistical and systematic errors. The systematic uncertainties are described in detail in [3, 4] and include energy dependent errors stemming from BDT stability, trigger efficiency in the low-energy region, tracking performance, dependence on charge and electron identification methods, and MC model dependence. The absolute energy scale was calibrated and shifted by $+3.5\%$ as a result of studies of the geomagnetic cutoff energy. From the Fig.1 it is possible to notice that the measurements of the electron flux are divided into two groups: AMS-02 + CALET and Fermi-LAT + DAMPE, with good consistency within each group, but with only marginal overlap between the two, possibly indicating the presence of unknown systematic errors. Although CALET and AMS-02 use different detection techniques their spectra are consistent below ~ 1 TeV where both experiments have a good electron identification capability. CALET observation of a flux suppression above ~ 1 TeV has now reached a significance $> 6.5\sigma$ and, in this region, it is found to be consistent with DAMPE within errors.

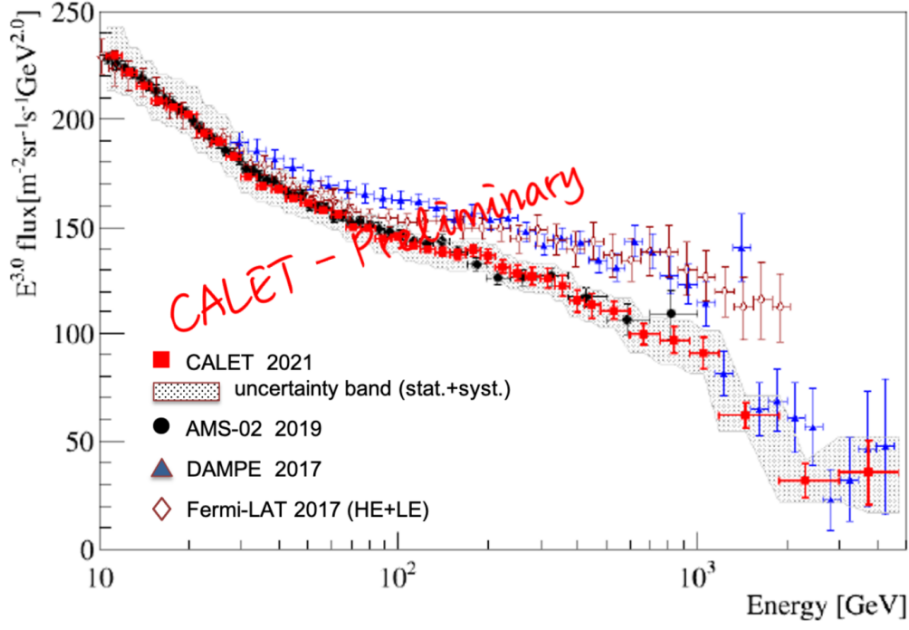


Figure 1: CALET all-electron flux (multiplied by $E^{3.0}$). The error bars of the CALET data (red) represent the statistical uncertainty only, the gray band indicates the the quadrature sum of statistical and systematic errors. Also plotted are other direct measurements. [5–7]

4.2 Precision Measurement of the Proton Spectrum

The measurement of the proton spectrum from 50 GeV to 60 TeV with CALET presented here is the published CALET proton spectrum [8], based on flight data collected for 2272 days from October 13, 2015, to December 31, 2021. The total observation live time with the HE shower trigger is 1925 days. A low-energy (LE) shower trigger, operated at high geomagnetic latitudes, was also used for the analysis of the low-energy region. In Fig.2 the CALET proton flux is compared with AMS-02 [9], CREAM-III[11], and DAMPE[10]. Below 200 GeV, the result is fully consistent. In the higher energy region, a systematic difference is observed, but the difference is within the errors. We confirm the presence of a spectral hardening around 500 GeV with a higher significance of more than 20σ (statistical error). We also observe a spectral softening around 10 TeV. In order to quantify the spectral hardening and softening, we fit the proton spectrum from 80 GeV to 60 TeV using a Double Broken Power Law (DBPL) function defined as follows:

$$\Phi'(E) = C \times \left(\frac{E}{1\text{GeV}} \right)^\gamma \times \phi(E) \quad (1)$$

where

$$\phi(E) = \left[1 + \left(\frac{E}{E_0} \right)^s \right]^{\frac{\Delta\gamma}{s}} \times \left[1 + \left(\frac{E}{E_1} \right)^{s_1} \right]^{\frac{\Delta\gamma_1}{s_1}} \quad (2)$$

where $\Phi'(E)$ is the proton flux, C is a normalization factor, γ the spectral index, E_0 is a characteristic energy of the region where a gradual spectral hardening is observed, $\Delta\gamma$ the spectral variation due to the spectral hardening, E_1 a characteristic energy of the transition to the region of spectral softening, and $\Delta\gamma_1$ is the spectral index variation observed above E_1 . Two independent smoothness

parameters s and s_1 are introduced in the energy intervals where spectral hardening and softening occur, respectively. In Fig.3, the black filled circles show the data with statistical errors and the red line shows the best fitted function with parameters $\gamma = -2.83^{+0.01}_{-0.02}$, $s = 2.4^{+0.8}_{-0.6}$, $\Delta\gamma = 0.28^{+0.04}_{-0.02}$, $E_0 = 584^{+61}_{-58}$ GeV, $\Delta\gamma_1 = -0.34^{+0.06}_{-0.06}$, $E_1 = 9.3^{+1.4}_{-1.1}$ TeV and $s_1 \sim 30$ with a large error. The χ^2 is 4.4 with 20 degrees of freedom.

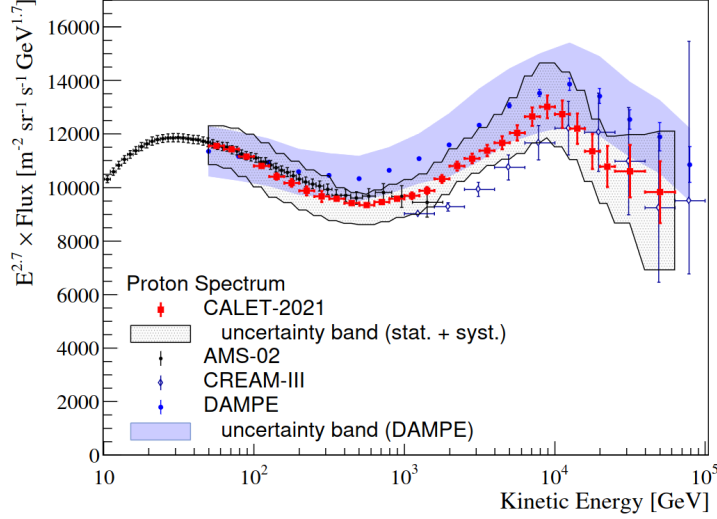


Figure 2: CALET proton flux (multiplied by $E^{2.7}$). The error bars of the CALET data (red) represent the statistical uncertainty only, the gray band indicates the the quadrature sum of statistical and systematic errors. Also plotted are other direct measurements. [9–11]

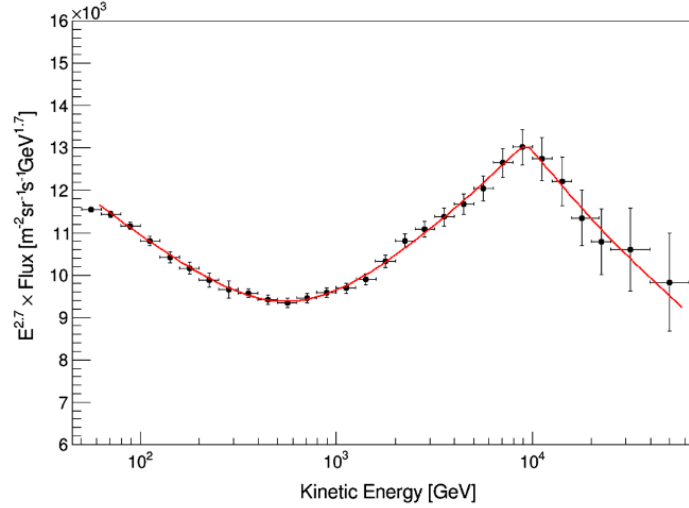


Figure 3: A fit of the CALET proton spectrum (solid red line) with a double broken power law (Eq.1). The horizontal error bars are representative of the bin width.

4.3 Precision Measurement of the Helium Spectrum

The measurement of the helium spectrum with CALET presented at this conference is the just published CALET helium spectrum [12] in an interval of kinetic energy per particle from 40 GeV to

250 TeV, based on flight data collected for 2392 days from October 13, 2015, to April 30, 2022. The energy spectrum of CR helium is shown in Fig.4 where the statistical and systematic uncertainties are bounded within a gray band. It is compared with previous observations from space-based [13, 14] and balloon-borne [11] experiments. CALET spectrum is in good agreement with AMS-02 in the lower energy region below a few TeV, as well as with the measurements from DAMPE in the higher energy region. In Fig.5, a fit of CALET data with a DBPL is shown in the energy range from 60 GeV to 250 TeV. The fit result gives $\gamma = -2.70^{+0.03}_{-0.01}$, $s = 2.7^{+3.0}_{-1.0}$, $\Delta\gamma = 0.25^{+0.03}_{-0.03}$, $E_0 = 1319^{+290}_{-155}$ GeV, $\Delta\gamma_1 = -0.22^{+0.08}_{-0.11}$, $E_1 = 33.3^{+10.0}_{-6.6}$ TeV. The second smoothness parameter is kept fixed at a value of $s_1 = 30$. The fit parameters are generally consistent, within the errors, with the recent results of DAMPE [13], although $\Delta\gamma_1$ seems to indicate a less pronounced softening in CALET data. The index change $\Delta\gamma$ is proven to be different from zero by more than 8σ , taking into account both statistical and systematic error.

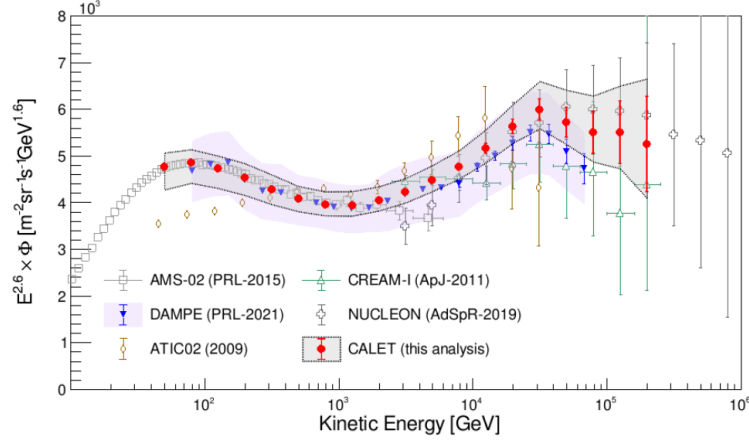


Figure 4: CALET helium flux (red markers), multiplied by $E^{2.6}$ and compared with previous direct observations [11, 13–16]. The error bars represent only the statistical error; the gray band represents the quadratic sum of statistical and systematic error.

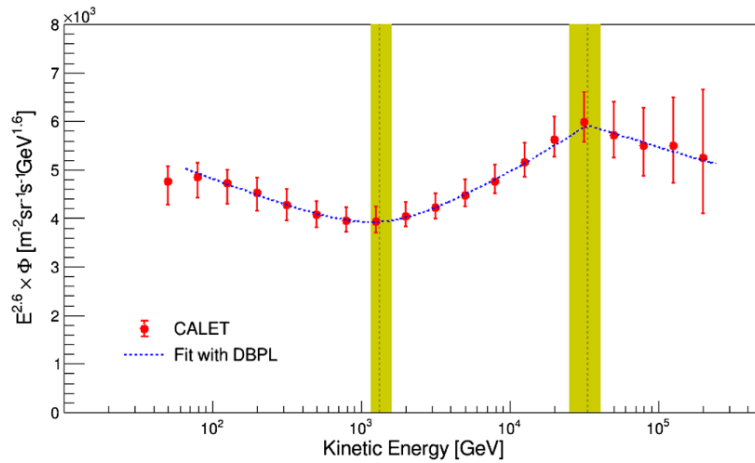


Figure 5: A fit of the CALET helium spectrum (dashed blue line) with a double broken power law. The vertical dashed lines represent the characteristic transition energy E_0 and E_1 to the region of spectral hardening and softening, respectively.

4.4 Proton to Helium ratio

Using the CALET proton flux [8], we also measured the proton over helium ratio in the interval from 60 GeV/n to 60 TeV/n. Owing to the partial cancellation of systematic errors in the ratio, this measurement can provide important information on the respective acceleration and propagation mechanisms. In Fig.6 (a) the p/He ratio is shown in kinetic energy per nucleon, together with the measurements from other experiments [11, 17]. The result is found to be in agreement with previous measurements from magnetic spectrometers [14, 18] up to their maximum detectable rigidity (~ 2 TV), as shown in Fig.6 (b).

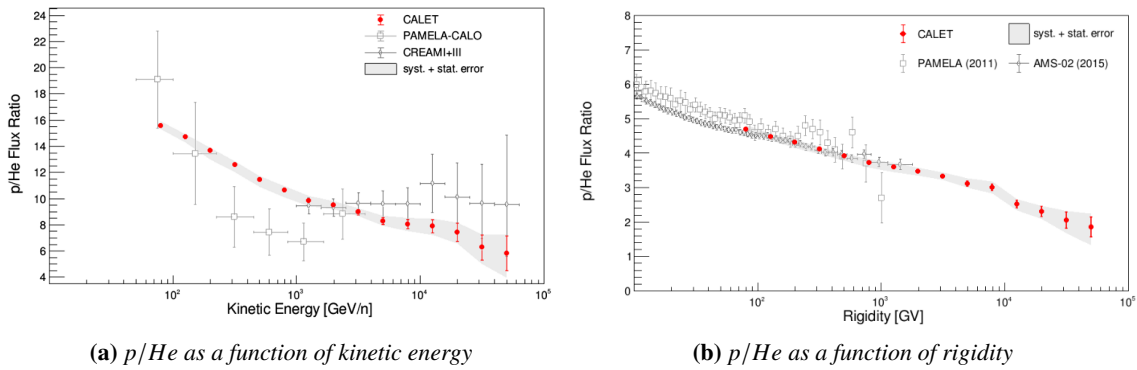


Figure 6: (a) The p/He ratio as measured by CALET as a function of kinetic energy; the red bars represent statistical error only; the gray band represents the quadratic sum of statistical and systematic errors. Results of previous measurements from CREAM [11] and PAMELA (calorimeter analysis) [17] are shown. (b) The p/He ratio as measured by CALET as a function of rigidity; the red vertical bars represent statistical error only, while the gray band represents the quadratic sum of statistical and systematic errors. Previous measurements from AMS-02 [14] and PAMELA [18] are shown.

4.5 Further CALET Observations

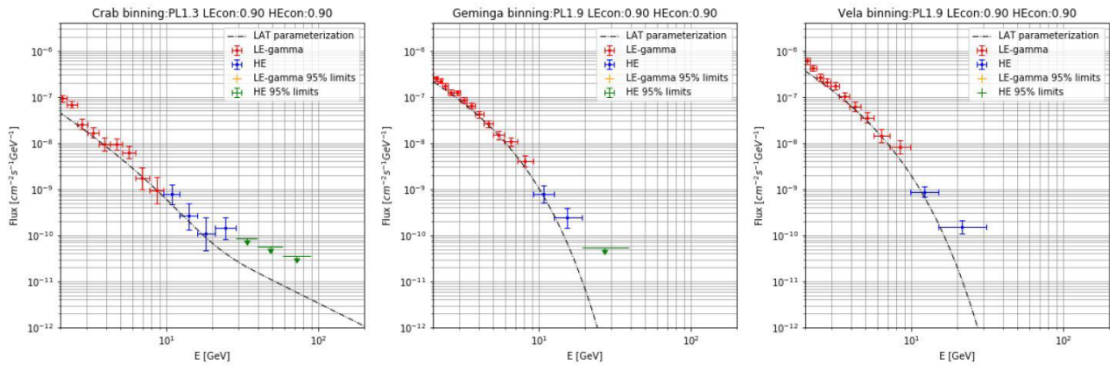
In addition to the results on CR nuclei spectra, CALET has also reported results on other aspects of cosmic rays, including the solar modulation [19], search for counterparts of gravitational waves [20, 21], Galactic and extra-galactic point sources [22], Galactic diffuse emission and dark matter line searches [23] and Solar and space weather phenomena [22].

4.5.1 Gamma-ray Transients, Search for counterparts of gravitational wave candidates

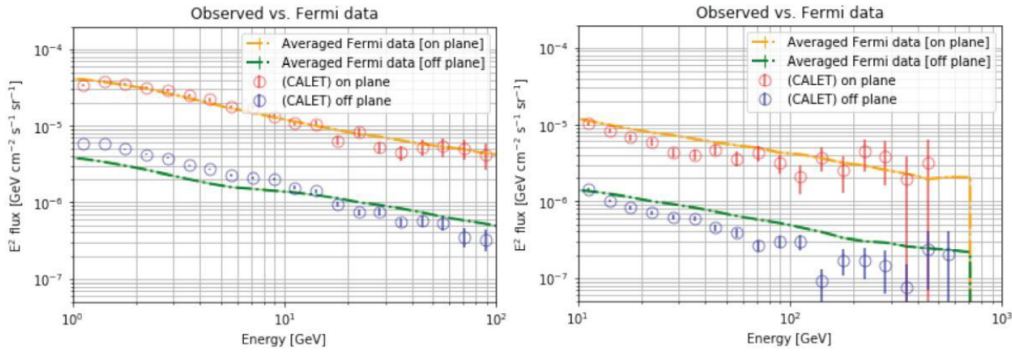
The CALET gamma-ray burst monitor (CGBM), designed to observe prompt emissions of gamma-ray bursts (GRBs) in the hard X-ray and soft gamma-ray band, has been providing all-sky monitoring, with $\sim 60\%$ duty cycle and without any problems, since October 2015. As of the end of January 2022, the CGBM has detected 314 GRBs, including 33 short GRBs. CALET has actively participated in the follow-up campaign for the search of electromagnetic counterparts of the gravitational wave events observed by LIGO/Virgo [20, 21]. Although no candidates have been found, upper limits on the high-energy gamma-ray flux were derived for 26 events from the LIGO/Virgo third observation run.

4.5.2 Gamma-rays observations

CALET is sensitive to gamma rays from 1 GeV up to 10 TeV, limited by statistics. Access to energies below 10 GeV is enabled by a dedicated low-energy gamma (LE- γ) trigger which is active only at low geomagnetic latitudes. Analyzing the CALET/CAL data acquired between November 2015 to December 2022 we identified 23 point sources in the skymaps Fig.8. The Fig.7 (a) shows the spectra of Crab, Geminga and Vela, compared with the parametrized spectra given by the Fermi-LAT collaboration [24, 25]. The spectra are consistent each other within statistical errors. The Fig.7 (b) shows comparison of the Galactic plane (diffuse plus discrete sources) spectra ($|b| < 8^\circ$) and the off-Galactic plane spectra ($|b| > 10^\circ$) taken with CALET and Fermi-LAT. The left panel shows a plot for LE- γ data and the right panel for HE data.



(a) Spectra of Crab, Geminga and Vela



(b) Galactic plane and the off-Galactic plane spectra

Figure 7: (a) Comparison of energy spectra of some point sources (Crab, Geminga and Vela) observed by CALET and parametrized spectra given by the Fermi-LAT collaboration [24, 25]. (b) The Galactic plane (diffuse plus point-sources) spectra ($|b| < 8^\circ$) and the off-Galactic plane spectra ($|b| > 10^\circ$) taken with CALET and Fermi-LAT. The left panel shows a plot for LE- γ data and the right panel for HE data.

5. Summary

CALET was successfully launched on August 19, 2015. The observation campaign started on October 13, 2015. Excellent performance and remarkable stability of the instrument were confirmed. The results presented in this paper are based on about 2700 days of observation and

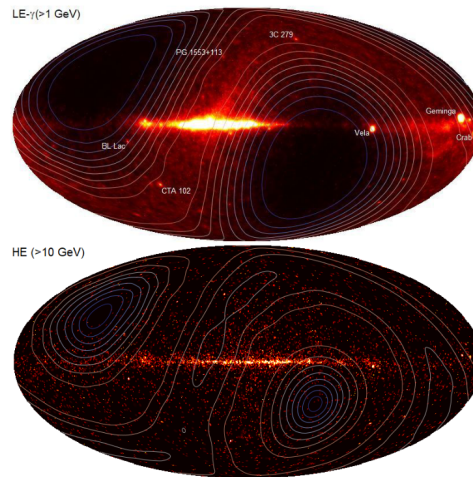


Figure 8: Skymaps showing gamma-ray intensities observed by CALET/CAL in galactic coordinates. The upper panel shows the skymap for LE- γ triggers (> 1 GeV) and the lower panel shows that for HE triggers (> 10 GeV). Superimposed contours show relative exposures.

~ 3.8 billion triggers (for energies > 1 GeV). They include an updated measurement of the electron and positron spectrum up to 4.8 TeV, the proton spectrum up to 60 TeV [8], the helium spectrum up to 250 TeV just published in 2023 [12] together with the cosmic-ray proton over helium ratio. CALET is also able to obtain precise measurements of the fluxes of CR nuclei from boron to nickel up to the TeV region [26–28] and secondary-to-primary ratios of individual elements [29]. Improved analyses of gamma-ray measurements [22, 23], GRB observations and searches of GW events counterparts [20, 21], DM searches [23], and Space Weather observations [22] are the subject of study for CALET. Extended CALET operations were approved by JAXA/NASA/ASI in March 2021 through the end of 2024 (at least). Improved statistics and refinement of the analysis with additional data collected during the lifetime of the mission will allow to extend the measurements at higher energies and improve the spectral analysis, contributing to a better understanding of CR phenomena.

References

- [1] CALET collaboration, *On-orbit operations and offline data processing of CALET onboard the ISS*, *Astroparticle Physics* **100** (2018) 29.
- [2] Y. Akaike, *Simulations for CALET Energy Calibration Confirmed Using CERN-SPS Beam Tests*, in *Proceedings of Science (ICRC2015)* 613, 2015.
- [3] O. Adriani et al., *Extended Measurement of the Cosmic-Ray Electron and Positron Spectrum from 11 GeV to 4.8 TeV with the Calorimetric Electron Telescope on the International Space Station*, *Phys. Rev. Lett.* **120** (2018) 261102.
- [4] O. Adriani et al., *Energy Spectrum of Cosmic-Ray Electron and Positron from 10 GeV to 3 TeV Observed with the Calorimetric Electron Telescope on the International Space Station*, *Phys. Rev. Lett.* **119** (2017) 181101.
- [5] M. Aguilar et al., *Towards Understanding the Origin of Cosmic-Ray Electrons*, *Phys. Rev. Lett.* **122** (2019) 101101.
- [6] G. Ambrosi et al., *Direct detection of a break in the teraelectronvolt cosmic-ray spectrum of electrons and positrons*, *Nature*. **552** (2017) 63.
- [7] S. Abdollahi et al., *Cosmic-ray electron-positron spectrum from 7 GeV to 2 TeV with the Fermi Large Area Telescope*, *Phys. Rev. D.* **95** (2017) 082007.
- [8] O. Adriani et al., *Observation of Spectral Structures in the Flux of Cosmic-Ray Protons from 50 GeV to 60 TeV with the Calorimetric Electron Telescope on the International Space Station*, *Phys. Rev. Lett.* **129** (2022) 101102.
- [9] M. Aguilar et al., *Precision Measurement of the Proton Flux in Primary Cosmic Rays from Rigidity 1 GV to 1.8 TV with the Alpha Magnetic Spectrometer on the International Space Station*, *Phys. Rev. Lett.* **114** (2015) 171103.
- [10] Q. An et al., *Measurement of the cosmic ray proton spectrum from 40 GeV to 100 TeV with the DAMPE satellite*, *Science Advanced* **5** (2019) 19.
- [11] Y. Yoon et al., *Proton and Helium Spectra from the CREAM-III Flight*, *Astrophys. J.* **839** (2017) 5.
- [12] O. Adriani et al., *Direct Measurement of the Cosmic-Ray Helium Spectrum from 40 GeV to 250 TeV with the Calorimetric Electron Telescope on the International Space Station*, *Phys. Rev. Lett.* **130** (2023) 171002.
- [13] F. Alemanno et al., *Measurement of the Cosmic Ray Helium Energy Spectrum from 70 GeV to 80 TeV with the DAMPE Space Mission*, *Phys. Rev. Lett.* **126** (2021) 201102.
- [14] M. Aguilar et al., *Precision Measurement of the Helium Flux in Primary Cosmic Rays of Rigidities 1.9 GV to 3 TV with the Alpha Magnetic Spectrometer on the International Space Station*, *Phys. Rev. Lett.* **115** (2015) 211101.
- [15] A. Panov et al., *Energy spectra of abundant nuclei of primary cosmic rays from the data of ATIC-2 experiment: Final results*, *Bull. Russian Acad. Sci.* **73** (2009) 564.

- [16] V. Grebenyuk et al., *Energy spectra of abundant cosmic-ray nuclei in the NUCLEON experiment*, *Adv. in Space Res.* **64** (2019) 2546.
- [17] O. Adriani et al., *Measurements of cosmic-ray proton and helium spectra with the PAMELA calorimeter*, *Adv. in Space Res.* **219** (2013) 51.
- [18] O. Adriani et al., *PAMELA Measurements of Cosmic-Ray Proton and Helium Spectra*, *Science* **332** (2011) 69.
- [19] O. Adriani et al., *Charge-Sign Dependent Cosmic-Ray Modulation Observed with the Calorimetric Electron Telescope on the International Space Station*, *Phys. Rev. Lett.* **130** (2023) 211001.
- [20] O. Adriani et al., *Search for GeV Gamma-ray Counterparts of Gravitational Wave Events by CALET*, *Astrophys. J.* **863** (2018) 160.
- [21] O. Adriani et al., *CALET Search for Electromagnetic Counterparts of Gravitational Waves during the LIGO/Virgo O3 Run*, *Astrophys. J.* **913** (2022) 85.
- [22] N. Cannady, *Low-energy gamma-ray observations above 1 GeV with CALET on the International Space Station*, in *Proceedings of Science (ICRC2021)* 604, 2021.
- [23] M. Mori, *High-energy gamma-ray observations above 10 GeV with CALET on the International Space Station*, in *Proceedings of Science (ICRC2021)* 609, 2021.
- [24] A.A. e et al., *Fermi large area telescope observations of the Crab pulsar and nebula*, *Astrophys. J.* **708** (2010) 1254.
- [25] A.A. e et al., *Fermi large area telescope observations of the Geminga pulsar*, *Astrophys. J.* **720** (2010) 272.
- [26] O. Adriani et al., *Direct Measurement of the Cosmic-Ray Carbon and Oxygen Spectra from 10 GeV/n to 2.2 TeV/n with the Calorimetric Electron Telescope on the International Space Station*, *Phys. Rev. Lett.* **125** (2020) 251102.
- [27] O. Adriani et al., *Measurement of the Iron Spectrum in Cosmic Rays from 10 GeV/n to 2 TeV/n with the Calorimetric Electron Telescope on the International Space Station*, *Phys. Rev. Lett.* **126** (2021) 241101.
- [28] O. Adriani et al., *Direct Measurement of the Nickel Spectrum in Cosmic Rays in the Energy Range from 8.8 GeV/n to 240 GeV/n with CALET on the International Space Station*, *Phys. Rev. Lett.* **128** (2022) 131103.
- [29] O. Adriani et al., *Cosmic-Ray Boron Flux Measured from 8.4 GeV/n to 3.8 TeV/n with the Calorimetric Electron Telescope on the International Space Station*, *Phys. Rev. Lett.* **129** (2022) 251103.

Full Author List: CALET Collaboration

O. Adriani^{1,2}, Y. Akaike^{3,4}, K. Asano⁵, Y. Asaoka⁵, E. Berti^{2,6}, G. Bigongiari^{7,8}, W.R. Binns⁹, M. Bonghi^{1,2}, P. Brogi^{7,8}, A. Bruno¹⁰, N. Cannady^{11,12,13}, G. Castellini⁶, C. Checchia^{7,8}, M.L. Cherry¹⁴, G. Collazuol^{15,16}, G.A. de Nolfo¹⁰, K. Ebisawa¹⁷, A.W. Ficklin¹⁴, H. Fuke¹⁷, S. Gonzi^{1,2,6}, T.G. Guzik¹⁴, T. Hams¹¹, K. Hibino¹⁸, M. Ichimura¹⁹, K. Ioka²⁰, W. Ishizaki⁵, M.H. Israel⁹, K. Kasahara²¹, J. Kataoka²², R. Kataoka²³, Y. Katayose²⁴, C. Kato²⁵, N. Kawanaka²⁰, Y. Kawakubo¹⁴, K. Kobayashi^{3,4}, K. Kohri²⁶, H.S. Krawczynski⁹, J.F. Krizmanic¹², P. Maestro^{7,8}, P.S. Marrocchesi^{7,8}, A.M. Messineo^{8,27}, J.W. Mitchell¹², S. Miyake²⁸, A.A. Moiseev^{29,12,13}, M. Mori³⁰, N. Mori², H.M. Motz¹⁸, K. Munakata²⁵, S. Nakahira¹⁷, J. Nishimura¹⁷, S. Okuno¹⁸, J.F. Ormes³¹, S. Ozawa³², L. Pacini^{2,6}, P. Papini², B.F. Rauch⁹, S.B. Ricciarini^{2,6}, K. Sakai^{11,12,13}, T. Sakamoto³³, M. Sasaki^{29,12,13}, Y. Shimizu¹⁸, A. Shiomi³⁴, P. Spillantini¹, F. Stolzi^{7,8}, S. Sugita³³, A. Sulaj^{7,8}, M. Takita⁵, T. Tamura¹⁸, T. Terasawa⁵, S. Torii³, Y. Tsunesada^{35,36}, Y. Uchihori³⁷, E. Vannuccini², J.P. Wefel¹⁴, K. Yamaoka³⁸, S. Yanagita³⁹, A. Yoshida³³, K. Yoshida²¹, and W.V. Zober⁹

¹Department of Physics, University of Florence, Via Sansone, 1 - 50019, Sesto Fiorentino, Italy, ²INFN Sezione di Firenze, Via Sansone, 1 - 50019, Sesto Fiorentino, Italy, ³Waseda Research Institute for Science and Engineering, Waseda University, 17 Kikuicho, Shinjuku, Tokyo 162-0044, Japan, ⁴JEM Utilization Center, Human Spaceflight Technology Directorate, Japan Aerospace Exploration Agency, 2-1-1 Sengen, Tsukuba, Ibaraki 305-8505, Japan, ⁵Institute for Cosmic Ray Research, The University of Tokyo, 5-1-5 Kashiwa-no-Ha, Kashiwa, Chiba 277-8582, Japan, ⁶Institute of Applied Physics (IFAC), National Research Council (CNR), Via Madonna del Piano, 10, 50019, Sesto Fiorentino, Italy, ⁷Department of Physical Sciences, Earth and Environment, University of Siena, via Roma 56, 53100 Siena, Italy, ⁸INFN Sezione di Pisa, Polo Fibonacci, Largo B. Pontecorvo, 3 - 56127 Pisa, Italy, ⁹Department of Physics and McDonnell Center for the Space Sciences, Washington University, One Brookings Drive, St. Louis, Missouri 63130-4899, USA, ¹⁰Heliospheric Physics Laboratory, NASA/GSFC, Greenbelt, Maryland 20771, USA, ¹¹Center for Space Sciences and Technology, University of Maryland, Baltimore County, 1000 Hilltop Circle, Baltimore, Maryland 21250, USA, ¹²Astroparticle Physics Laboratory, NASA/GSFC, Greenbelt, Maryland 20771, USA, ¹³Center for Research and Exploration in Space Sciences and Technology, NASA/GSFC, Greenbelt, Maryland 20771, USA, ¹⁴Department of Physics and Astronomy, Louisiana State University, 202 Nicholson Hall, Baton Rouge, Louisiana 70803, USA, ¹⁵Department of Physics and Astronomy, University of Padova, Via Marzolo, 8, 35131 Padova, Italy, ¹⁶INFN Sezione di Padova, Via Marzolo, 8, 35131 Padova, Italy, ¹⁷Institute of Space and Astronautical Science, Japan Aerospace Exploration Agency, 3-1-1 Yoshinodai, Chuo, Sagami-hara, Kanagawa 252-5210, Japan, ¹⁸Kanagawa University, 3-27-1 Rokkakubashi, Kanagawa, Yokohama, Kanagawa 221-8686, Japan, ¹⁹Faculty of Science and Technology, Graduate School of Science and Technology, Hirosaki University, 3, Bunkyo, Hirosaki, Aomori 036-8561, Japan, ²⁰Yukawa Institute for Theoretical Physics, Kyoto University, Kitashirakawa Oiwake-cho, Sakyo-ku, Kyoto, 606-8502, Japan, ²¹Department of Electronic Information Systems, Shibaura Institute of Technology, 307 Fukasaku, Minuma, Saitama 337-8570, Japan, ²²School of Advanced Science and Engineering, Waseda University, 3-4-1 Okubo, Shinjuku, Tokyo 169-8555, Japan, ²³National Institute of Polar Research, 10-3, Midori-cho, Tachikawa, Tokyo 190-8518, Japan, ²⁴Faculty of Engineering, Division of Intelligent Systems Engineering, Yokohama National University, 79-5 Tokiwadai, Hodogaya, Yokohama 240-8501, Japan, ²⁵Faculty of Science, Shinshu University, 3-1-1 Asahi, Matsumoto, Nagano 390-8621, Japan, ²⁶Institute of Particle and Nuclear Studies, High Energy Accelerator Research Organization, 1-1 Oho, Tsukuba, Ibaraki, 305-0801, Japan, ²⁷University of Pisa, Polo Fibonacci, Largo B. Pontecorvo, 3 - 56127 Pisa, Italy, ²⁸Department of Electrical and Electronic Systems Engineering, National Institute of Technology (KOSEN), Ibaraki College, 866 Nakane, Hitachinaka, Ibaraki 312-8508, Japan, ²⁹Department of Astronomy, University of Maryland, College Park, Maryland 20742, USA, ³⁰Department of Physical Sciences, College of Science and Engineering, Ritsumeikan University, Shiga 525-8577, Japan, ³¹Department of Physics and Astronomy, University of Denver, Physics Building, Room 211, 2112 East Wesley Avenue, Denver, Colorado 80208-6900, USA, ³²Quantum ICT Advanced Development Center, National Institute of Information and Communications Technology, 4-2-1 Nukui-Kitamachi, Koganei, Tokyo 184-8795, Japan, ³³College of Science and Engineering, Department of Physics and Mathematics, Aoyama Gakuin University, 5-10-1 Fuchinobe, Chuo, Sagami-hara, Kanagawa 252-5258, Japan, ³⁴College of Industrial Technology, Nihon University, 1-2-1 Izumi, Narashino, Chiba 275-8575, Japan, ³⁵Graduate School of Science, Osaka Metropolitan University, Sugimoto, Sumiyoshi, Osaka 558-8585, Japan, ³⁶Nambu Yoichiro Institute for Theoretical and Experimental Physics, Osaka Metropolitan University, Sugimoto, Sumiyoshi, Osaka 558-8585, Japan, ³⁷National Institutes for Quantum and Radiation Science and Technology, 4-9-1 Anagawa, Inage, Chiba 263-8555, Japan, ³⁸Nagoya University, Furo, Chikusa, Nagoya 464-8601, Japan, ³⁹College of Science, Ibaraki University, 2-1-1 Bunkyo, Mito, Ibaraki 310-8512, Japan